Dark matter microphysics and 21 cm observations

Laura Lopez-Honorez,[1,2,*] Olga Mena,[3,†] and Pablo Villanueva-Domingo[3,‡]
[1]Service de Physique Théorique, CP225, Université Libre de Bruxelles, Bld du Triomphe, 1050 Brussels, Belgium
[2]Vrije Universiteit Brussel and The International Solvay Institutes, Pleinlaan 2, 1050 Brussels, Belgium
[3]Instituto de Física Corpuscular (IFIC), CSIC-Universitat de Valencia, Apartado de Correos 22085, E-46071, Spain

(Received 20 November 2018; published 22 January 2019)

Dark matter interactions with massless or very light standard model particles, as photons or neutrinos, may lead to a suppression of the matter power spectrum at small scales and of the number of low mass haloes. Bounds on the dark matter scattering cross section with light degrees of freedom in such interacting dark matter (IDM) scenarios have been obtained from e.g., early time cosmic microwave background physics and large scale structure observations. Here we scrutinize dark matter microphysics in light of the claimed 21 cm EDGES 78 MHz absorption signal. IDM is expected to delay the 21 cm absorption features due to collisional damping effects. We identify the astrophysical conditions under which the existing constraints on the dark matter scattering cross section could be largely improved due to the IDM imprint on the 21 cm signal, providing also an explicit comparison to the WDM scenario.

DOI: 10.1103/PhysRevD.99.023522

I. INTRODUCTION

Interacting dark matter (IDM) with standard model light or massless degrees of freedom, such as photons and neutrinos, gives rise to a suppression of the small-scale matter power spectrum [1–4] (see also Refs. [5–12] for interactions with new (dark) light degrees of freedom). This damping is similar to the one caused by the free streaming of warm dark matter (WDM). In IDM scenarios, in contrast, the suppression of the small-scale overdensities is due to collisional damping [13–15]. These two alternatives to the standard ΛCDM model fall into the category of *noncold dark matter* scenarios [16] (NCDM). Such dark matter models can provide some solutions to the ΛCDM (where dark matter is made of purely cold and collisionless dark matter particles) *small scale crisis* (see, e.g., the review of Ref. [17]). A large number of studies in the literature have been devoted to constrain the NCDM picture by means of cosmological probes, such as cosmic microwave background (CMB) fluctuations and spectral distortions, galaxy clustering and Lyman-α forest power spectrum, the number of Milky Way satellites, the reionization history, or gravitational lensing [1–4,15,16,18–65].

In this regard, the 21 cm signal offers a new cosmological probe, complementary to the existing ones, that could open a new window on the early universe and can further test the imprint of NCDM (see, e.g., [66,67] for early work on the subject). Here we will focus on the cosmic dawn period and in particular on the first claimed detection of an absorption feature in the sky-averaged global 21 cm signal at a redshift $z \sim 17$ by the experiment to Detect the Global Epoch of Reionization Signatures (EDGES) [68]. The measured amplitude of the dip in the 21 cm global signal appears to be much deeper than that expected in standard CDM scenarios and therefore requires new physics to heat the radio background or cool the gas temperature. This has triggered a surge of interest from the dark matter community trying to relate this effect to dark matter decay and annihilation [69–72][1] and investigating the dark matter scenarios that could account for the signal [76–81], see also [82–84]. There are however other possible interpretations of the EDGES signal that do not involve new physics. In particular, the signal could be explained with a different modeling of the foregrounds [85] or with the existence of a systematic artifact within the ground plane which may also produce an absorption feature [86].

While NCDM scenarios are unlikely to explain the large absorption amplitude, they delay structure formation and, therefore, might delay the onset of reionization and of UV and x-ray emission, see e.g., [45,46,60,66]. As a result a shift to later times in the typical features in the 21 cm sky-averaged global signal and power spectrum is observed in the context of non-cold dark matter [60,66,87–89]. Consequently, it is timely to study the compatibility

*llopezho@ulb.ac.be
†olga.mena@ific.uv.es
‡pablo.villanueva@ific.uv.es

[1]See also the previous works of Refs. [73–75].

between the observation reported by EDGES, located at a redshift around $z \simeq 17$ and the IDM scenario. We follow two possible avenues. The first of them relies on exploiting the non-negligible Lyman-α coupling between the gas and the spin temperature characterizing the 21 cm signal at $z \simeq 20$ [88,89]. The second one consists in imposing the minimum in the absorption feature to happen before $z \simeq 17$ [87]. For both strategies, a number of degeneracies between the details of dark matter microphysics and the astrophysical parameters will appear. We will briefly discuss their impact on the constraints on NCDM scenarios.

Universal fits to the halo mass functions from N-body simulations for the IDM scenarios have been obtained in [3,90,91]. In particular, here we will use the results of [90] derived for IDM scenarios involving dark matter-photon scatterings. A possible particle physics model related to this cosmological scenario is the case of millicharged dark matter [65,92,93]. IDM scenarios including dark matter-neutrino scatterings have been shown to give rise to a very similar damping in the power spectrum and also to a very similar mass function as for dark matter-photon scatterings, see Refs. [3,14] and the Appendix A. Unfortunately, in the latter case, no publicly available dedicated analysis provides the necessary fits to the associated halo mass functions necessary for our study. We therefore use the IDM scattering on photons as a toy model to evaluate the impact of the EDGES signal on the more general case of IDM with light degrees of freedom. In order to ease comparison with previous studies, we shall also study the case of thermal warm dark matter (WDM) with mass in the keV range (see Refs. [35,36,44–59,94–112] and the most recent works of Refs. [87,89]).

The structure of the paper is as follows. We start in Sec. II by describing the physics of the 21 cm global signature. We account for the effect of IDM in the 21 cm global signature in Sec. III, presenting the constraints on the dark matter photon elastic cross sections arising from (i) the presence of a rich Lyman-α background at $z \simeq 20$ (see Sec. III A), and (ii) the location of the EDGES minimum (see Sec. III B). Finally, we summarize our results and conclude in Sec. IV.

II. THE 21 CM SIGNAL

A. The differential brightness temperature

The brightness of a patch of neutral hydrogen (HI) relative to the CMB at a given redshift z is expressed in terms of the differential brightness temperature, δT_b. The sky-averaged δT_b scales as [113–116]

$$\frac{\delta T_b(\nu)}{\mathrm{mK}} \simeq 27 x_{\mathrm{HI}} \left(1 - \frac{T_{\mathrm{CMB}}}{T_{\mathrm{S}}}\right) \left(\frac{1+z}{10}\right)^{1/2} \times \left(\frac{0.15}{\Omega_m h^2}\right)^{1/2} \left(\frac{\Omega_b h^2}{0.023}\right), \tag{2.1}$$

where $\nu = \nu_{21}/(1+z)$ with $\nu_{21} = 1420$ MHz, x_{HI} represents the fraction of neutral hydrogen and $\Omega_b h^2$ and $\Omega_m h^2$ refer to the current baryon and matter contributions to the universe's mass-energy content. The ratio of the populations of the two ground state hyperfine levels of hydrogen is quantified by the spin temperature, T_{S}, which is determined by three competing effects [117]: (1) absorption and stimulated emission of CMB photons coupling the spin temperature to the CMB temperature T_{CMB} in contrast with (2) atomic collisions (which are important at high redshifts $z \gtrsim 30$); and 3) resonant scattering of Lyman-α photons that couple the spin temperature to the gas kinetic temperature T_k. The latter effect is the so-called Wouthuysen-Field effect [118,119] that turns on with the first sources. Assuming that the Lyman-α color temperature is $T_\alpha \simeq T_k$ [115], the spin temperature results from:

$$\left(1 - \frac{T_{\mathrm{CMB}}}{T_{\mathrm{S}}}\right) = \frac{x_{\mathrm{tot}}}{1 + x_{\mathrm{tot}}} \left(1 - \frac{T_{\mathrm{CMB}}}{T_k}\right) \tag{2.2}$$

with $x_{\mathrm{tot}} = x_\alpha + x_c$ and x_c and x_α are the coupling coefficients for collisions and Lyman-α scatterings.

At the low redshifts of interest here, collision coupling effects can be safely neglected and therefore, $x_{\mathrm{tot}} = x_\alpha$. The Lyman-$\alpha$ coupling is defined as

$$x_\alpha = \frac{16\pi^2 T_\star e^2 f_\alpha}{27 A_{10} T_\gamma m_e c} S_\alpha J_\alpha, \tag{2.3}$$

where $T_\star = h\nu_{21} = 68.2$ mK is the hyperfine energy splitting, e and m_e the charge and mass of the electron, f_α is the oscillator strength of the Lyman-α transition, A_{10} is the spontaneous decay rate of the 21 cm transition, J_α is the specific intensity of the background radiation evaluated at the Lyman-α frequency and S_α is an order unity correction factor which accounts for the detailed shape of the spectrum near the resonance [120]. In particular, in the framework considered here, $S_\alpha \lesssim 1$ and the Lyman-α flux gets two types of contributions. One results from the x-ray excitation of HI ($J_{\alpha X}$), while the other one results from direct stellar emission of UV photons between Lyman-α and the Lyman-α limit $J_{\alpha\star}$, thus $J_\alpha = J_{\alpha X} + J_{\alpha\star}$ [121]. We will see in Sec. II B that for the x-ray efficiencies considered here, $J_{\alpha X}$ only represents a small contribution to the total Lyα flux. On the other hand, the direct stellar emission contribution to J_α is computed assuming by default a Pop II stars spectral model. This gives rise to the emission of 9690 photons per baryon between Lyman-α and the Lyman limit, see Appendix B (see also [122]). Notice from Eq. (2.2) that, when $x_{\mathrm{tot}} = x_\alpha = 1$, δT_b will be at the half of the value that it would have if T_S were completely coupled to T_k, which happens when $x_\alpha \gg 1$. The authors of Ref. [89], following the EDGES results [68], have imposed that x_α should be one or larger at redshift $z \simeq 20$. We shall apply this constraint in our numerical analyses of IDM scenarios, see Sec. III A.

In order to extract the imprint of NCDM on the 21 cm signal, we profit from the publicly available tool 21CMFAST. The main purpose of the code is the study of variations in the 21 cm signal due to changes in a given set of astrophysical and cosmological parameters. We make use of the output values of x_α and of T_S and $x_{\rm HI}$ to extract the differential brightness temperature as in Eq. (2.1). We perform our simulations in a box of 300 Mpc of size with a 128^3 grid, since high-resolution computations are not required for extracting only the global 21 cm signal. In practice, we use a version of the 21CMFAST code adapted to account for the IDM and the WDM as detailed in Ref. [60]. We have modified the default WDM scenario implementation modifying the definition of both the transfer function and the halo mass function according to the prescription given in the Appendix A. This halo mass function plays an important role in the evaluation of the production rate of ultraviolet (UV), x-rays, and Lyman-α radiation, responsible of the ionization, heating and Lyman-α coupling respectively. These production rates are proportional to the star formation rate $\dot{\rho}_\star$. In 21CMFAST, this quantity is evaluated in terms of the growth of the fraction of mass collapsed in haloes which are able to host star-forming galaxies, $f_{\rm coll}(> M_{\rm vir}^{\rm min})$, defined as

$$f_{\rm coll}(> M_{\rm vir}^{\rm min}) = \frac{1}{\rho_{m,0}} \int_{M_{\rm vir}^{\rm min}}^{\infty} M \frac{dn}{dM} dM, \qquad (2.4)$$

where $\rho_{m,0}$ is the current matter density and dn/dM is the halo mass function. For the NCDM cosmologies, the halo mass function is always suppressed at small masses compared to the CDM scenario, giving rise to a smaller $f_{\rm coll}$, at fixed redshift, as illustrated in Fig. 1, see also [1,66,123].[2] With the purple area we show the case of CDM with threshold masses $M_{\rm vir}^{\rm min}$ between $10^6\ M_\odot$ (upper curve) and $3\times10^7\ M_\odot$ (lower curve) at $z = 20$ or equivalently $T_{\rm vir}^{\rm min}$ between 10^3 and 10^4 K, see Eq. (2.5). The upper purple curve for CDM can be compared to case of NCDM scenarios in the form of WDM (red, blue, and cyan continuous curves) and of IDM (red, blue, and cyan dotted curves) for the same $M_{\rm vir}^{\rm min} = 10^6\ M_\odot$ at $z = 20$ ($T_{\rm vir}^{\rm min} = 10^3$ K). The IDM scattering cross sections are normalized in terms of the Thompson cross section $\sigma_T = 6.65\times10^{-25}$ cm^2.

Overall, in the framework considered here, the NCDM modification of $f_{\rm coll}$ will result into a delayed reionization, heating and Lyman-α coupling, giving rise to an absorption feature in the 21 cm signal located at lower redshifts with respect to CDM scenarios [45,46,60,66]. Notice also that

[2]Let us emphasize that our prescription for WDM differs from one of [66]. Here we follow the fits to the results of simulations from [100] for WDM which was directly compared to the results of IDM simulations in [3,91,124]. Reference [66] followed an earlier prescription introduced by [47].

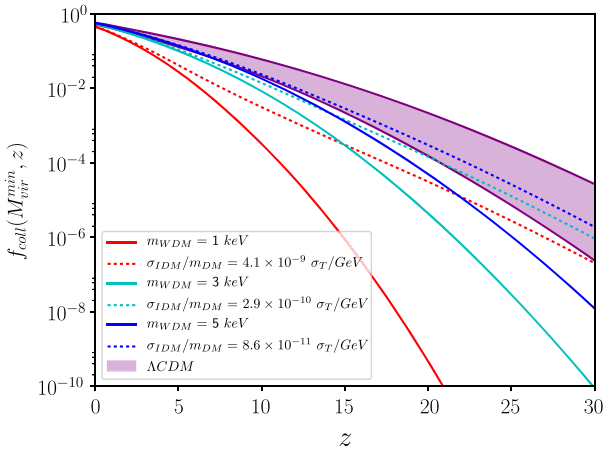

FIG. 1. Fraction of mass collapsed into haloes of mass larger than $M_{\rm vir}^{\rm min}(z = 20) \simeq 10^6\ M_\odot$ (corresponding to $T_{\rm vir}^{\rm min} = 10^3$ K) as a function of the redshift. The continuous lines depict the WDM cases that are compared with IDM scenarios, shown with dotted curves. Continuous and dotted curves of the same colors correspond to a fixed value of the half-mode mass. The purple region illustrates the change in the CDM collapsed fraction (using the Sheth-Tormen mass function) for $T_{\rm vir}^{\rm min}$ varying within the range of 10^3 to 10^4 K.

curves of a fixed color in Fig. 1 correspond to IDM and WDM models giving rise to a fixed value of the half-mode mass or breaking scale of the linear power spectrum, see Eqs. (A6), (A7), and (A9) in Appendix A. For fixed half-mode mass, the suppression of the $f_{\rm coll}$ is always more severe in the WDM scenarios than in the IDM scenarios due to a relatively larger number of low mass haloes in the IDM case, see [90]. The rate at which $f_{\rm coll}$ increases with redshift is also different between IDM and WDM. These features might help to discriminate between NCDM models using both the 21 cm global signal and its power spectrum [60].

B. The astrophysical parameters

The minimum virial mass $M_{\rm vir}^{\rm min}$ from which haloes begin to efficiently form stars [see Eq. (2.4)] is related to the threshold temperature $T_{\rm vir}^{\rm min}$ as [125]

$$M_{\rm vir}^{\rm min}(z) = 10^8 \left(\frac{T_{\rm vir}^{\rm min}}{1.98\times10^4\ {\rm K}} \frac{0.6}{\mu}\right)^{3/2} \left(\frac{1+z}{10}\right)^{-3/2} M_\odot/h, \qquad (2.5)$$

where μ is the mean molecular weight and it is equal to 1.2 (0.6) for a neutral (fully ionized) primordial gas. The value of the minimum virial temperature depends on the cooling mechanism considered. The lower threshold to make the atomic cooling channel effective is $T_{\rm vir}^{\rm min} = 10^4$ K [126–130], corresponding to $M_{\rm vir}^{\rm min} = 3\times10^7\ M_\odot$ at $z = 20$ for $\mu = 0.6$. In contrast, the molecular H_2 cooling channel can be effective down to temperatures of $T_{\rm vir}^{\rm min} = 10^3$ K

corresponding to $M_{\rm vir}^{\rm min} = 10^6\ M_\odot$ at $z = 20$. The hydrogen molecules could be destroyed by photons in the Lyman-Werner band. Nevertheless, several hydrodynamical works in the literature [131,132] have shown that in the presence of a large soft UV background, molecular cooling could be highly effective, i.e., metal-enriched star formation is not restricted to atomic cooling. Furthermore, molecular cooling could cool down the gas in haloes associated to virial temperatures much lower than the ones required for atomic cooling. Consequently, in the following, we shall consider $T_{\rm vir}^{\rm min} = 10^3$ K as the minimum threshold temperature for star formation and we assume the same threshold temperature $T_{\rm vir}^{\rm min}$ for haloes hosting ionizing and x-ray sources. This parameter plays a crucial role in extracting the constraints from the 21 cm absorption signal in both CDM and NCDM scenarios, see also [87,88]. The impact of varying $T_{\rm vir}^{\rm min}$ in the 10^3 K to 10^4 K range within the CDM paradigm is illustrated in Fig. 1 with the purple area. The lower value of the threshold parameter corresponds to higher values of the faction of collapsed haloes at a given redshift.

The comoving star formation rate density is described by $\dot{\rho}_\star = f_* \rho_{b,0} \dot{f}_{\rm coll}(> M_{\rm vir}^{\rm min})$, where f_*, the fraction of baryons that are converted into stars, considered here as a constant parameter (neglecting any dependence on the halo masses or redshift). As f_* controls the amplitude of the star formation rate density, it also sets the amplitude of both the ionizing and heating rates, as well as the Lyman-α flux. This parameter is quite uncertain as no observations of low mass haloes of mass $10^6 - 10^8\ M_\odot$ at redshift $z \sim 20$ are available. Nevertheless, several previous works, based on radiation-hydrodynamic simulations of high-redshift galaxies in a neutral medium [132–135] or based on the comparison of the star formation rate density to the one derived from UV luminosity function measurements [89,136,137], have found values of $f_* \sim \mathcal{O}(0.01)$. In the following, we therefore consider $f_* = 0.01$, leaving for the discussion in Sec. IV the impact in our results of slightly larger values of f_*.

Finally, in order to characterize the overall normalization of the x-ray luminosity, 21CMFAST makes use of the x-ray efficiency parameter ζ_X, expressed in units of $M_\odot^{-1}$. This parameter is varied here within the range $\zeta_X = [1\text{–}5] \times 10^{56}/M_\odot$. One can relate this parameter to the integrated x-ray soft band emissivity (below 2 keV) per unit of star formation rate escaping the galaxy $L_{X<2\,\rm keV}/\mathrm{SFR}$, varied in the range $\log_{10}(L_{X<2\,\rm keV}/\mathrm{SFR}) \in [39.5, 40.2]$ erg/s/$(M_\odot/\mathrm{yr})$.[3] This range is similar to one extracted from observations of the hot interstellar medium, which lead to $\log_{10}(L_{X<2\rm keV}/\mathrm{SFR}) \sim [39,40]$ erg/s/$(M_\odot/\mathrm{yr})$ [139], and also to the one adopted in Ref. [87] (see also Ref. [140]).

[3]The emissivity $L_{X<2\,\rm keV}/\mathrm{SFR}$ corresponds to the following combination of parameters: $\alpha_X \zeta_X h_p \int (\nu/\nu_0)^{-\alpha_X} d\nu$ where h_p is the Planck constant, α_X is the spectral slope parameter and ν_0 is the obscuration frequency cutoff parameter (see the 21CMMC code [138] based on 21CMFAST). The integral goes from ν_0 to 2 keV. We took $\alpha_X = 1.2$ and $\nu_0 = 7.2 \times 10^{12}$ Hz (corresponding to an energy of 300 eV), that are the default values in the 21CMFAST code.

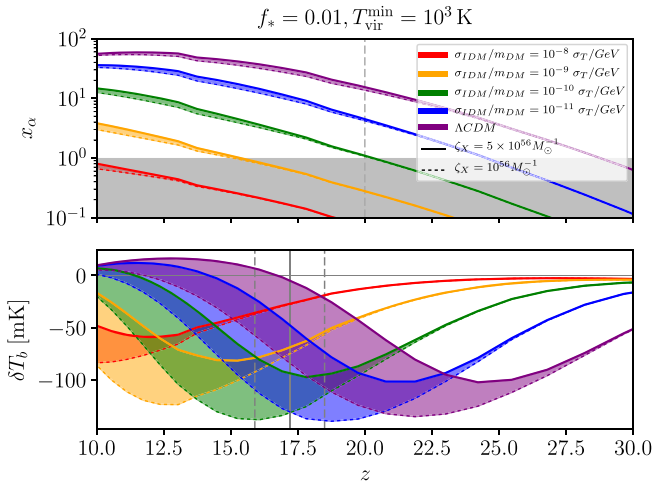

FIG. 2. Coupling coefficient for Lyman-α scattering (top) and sky-averaged 21 cm brightness temperature (bottom) as a function of the redshift for several possible values of the scattering dark matter-photon cross section over the dark matter particle mass. We have fixed $f_* = 0.01$ and $T_{\rm vir}^{\rm min} = 10^3$ K. The width of the bands refers to the change in δT_b and x_α due to different values of ζ_X.

III. IMPRINT OF THE IDM ON THE 21 CM SIGNAL

Noncold dark matter scenarios are expected to delay structure formation and therefore the absorption feature in the 21 cm signal at cosmic dawn. This effect is illustrated for the IDM model under study in Fig. 2, where we show the coupling coefficient for Lyman-α scattering x_α (top), and the sky-averaged 21 cm brightness temperature (bottom). The different colors correspond to different values of the dark matter-photon scattering cross sections over the dark matter particle mass, $\sigma_{\rm IDM}/\sigma_T(\mathrm{GeV}/m_{\rm DM})$. As can be noticed, large cross sections, inducing a stronger suppression at small scales, also induce a stronger suppression of the Lyman-α coupling at a given redshift (see the top panel of Fig. 2) and a larger shift toward smaller redshifts of the 21 cm features (see the bottom panel of Fig. 2). We also illustrate, with a vertical line, the position of the minimum of absorption reported by the EDGES experiment (at $\nu = 78$ MHz corresponding to $z = 17.2$). The dashed lines correspond to the largest signal redshift range at the minimum of absorption within the 99% CL interval reported by Ref. [68].

Figure 2 also shows the impact of varying the x-ray heating efficiency ζ_X in the $10^{56}\ M_\odot^{-1} - 5 \times 10^{56}\ M_\odot^{-1}$ range with the width of the colored bands. We see from the top panel of Fig. 2 that the range of ζ_X considered here, the Lyman-α flux resulting from x-ray excitation

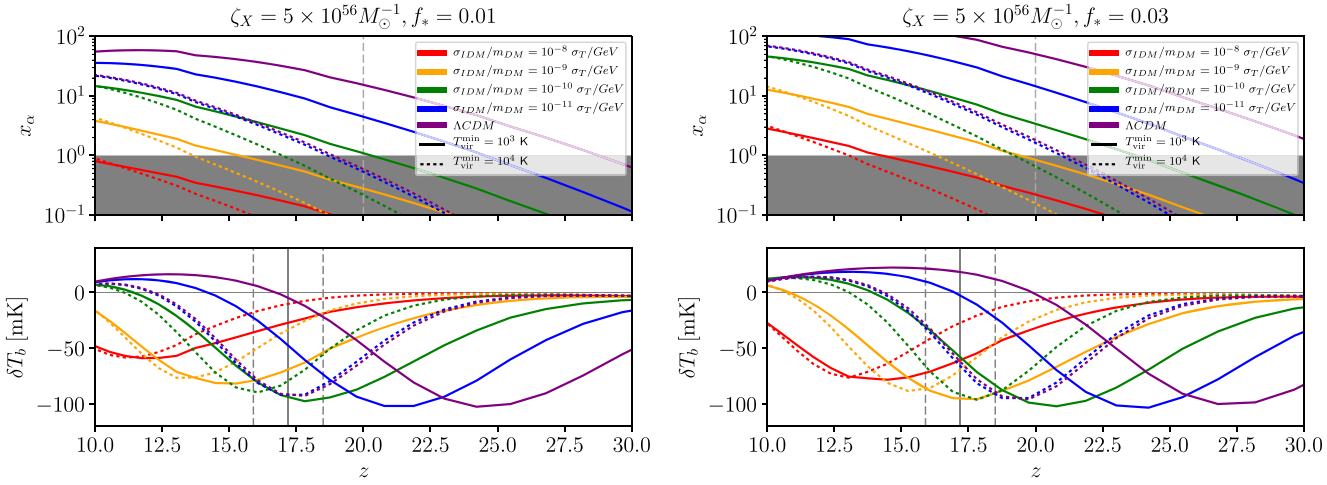

FIG. 3. Top panels: Lyman-α coupling coefficient x_α versus redshift for different values of the astrophysical parameter $T_{\rm vir}^{\rm min}$ and for several possible values of the scattering dark matter-photon cross-section over the dark matter mass. Cases within the shaded region are highly disfavoured by the condition given by Eq. (3.1). Bottom panels: sky-averaged 21 cm brightness temperature. The solid (dashed) lines indicates the mean redshift (range in redshift) associated to the EDGES signal. We have fixed $\zeta_X = 5 \times 10^{56}\ M_\odot$ and $f_* = 0.01$ ($f_* = 0.03$) in left (right) panel.

($J_{\alpha X} \propto \zeta_X$) is usually a negligible contribution to the Lyman-α coupling at the redshift at which $x_\alpha \sim 1$. On the bottom panel of Fig. 2, we see the impact of the x-ray heating parameter ζ_X on the differential brightness temperature. Here the impact is more significant. The deepest absorption dip corresponds to $\zeta_X = 10^{56}\ M_\odot^{-1}$, while the shallowest one is obtained for $\zeta_X = 5 \times 10^{56}\ M_\odot^{-1}$. Notice also that a larger value of ζ_X implies an earlier minimum, i.e., the x-ray heating of the IGM occurs earlier in time. As a result, in order to extract conservative constraints on the NCDM parameters from the redshift at which the absorption minimum is located, we shall consider the value $\zeta_X = 5 \times 10^{56}/M_\odot$, see Sec. III B. Even if a larger value of the x-ray efficiency parameter will make harder to match the observed depth of the EDGES signal, we recall here that our analyses are driven by the location (and not the amplitude) of the dip.

Figure 3 illustrates the equivalent to Fig. 2 with ζ_X fixed to $5 \times 10^{56}\ M_\odot^{-1}$ and considering this time $T_{\rm vir}^{\rm min} = 10^3$ K (continuous curves) as well as $T_{\rm vir}^{\rm min} = 10^4$ K (dotted curves). Going from left to right panel of Fig. 3 we increase the value of f_* by a factor of 3. Based on these plots, we discuss in the next two subsections the constraints that could be derived on NCDM scenarios following two different approaches. Notice that none of our predictions in Figs. 2 and 3 show the flat bottom present in the EDGES signal (see, e.g., Fig. 1 of [68]). Instead, these models have a more gradual evolution around the minimum. Together with the fact that we are unable to obtain the amplitude of 500 mK of the EDGES absorption dip, this shows that standard astrophysical predictions, even within NCDM models, cannot reproduce all the features of the EDGES profile, see, e.g., [141,142] for more details.

A. Constraints from the Lyman-α background

In order to account for the EDGES results, the authors of Ref. [89] based their analyses on the assumption that a sufficiently strong Lyman-α background is present by $z \sim 20$. They imposed

$$x_\alpha(z = 20) \gtrsim 1. \tag{3.1}$$

This limit results from the observation that the absorption signal reported by the EDGES experiment is equal to half of the maximum amplitude of absorption at $z \simeq 20$. We shall follow this assumption here, applying this condition to our simulations within NCDM models. Let us first focus on the top left panel of Fig. 3, which shows the Lyman-α coupling coefficient x_α as a function of the redshift for $f_* = 0.01$. The condition reported in (3.1) disfavors the cosmological scenarios associated to a prediction of $x_\alpha(z)$ lying within the shaded area at $z = 20$.

The astrophysical parameter $T_{\rm vir}^{\rm min}$ has a significant impact on the Lyman-α coupling coefficient x_α. Larger virial temperature shifts star formation to lower redshifts, giving rise to a lower Lyman-α background at a given redshift. In a similar way, a large value of the IDM scattering cross section implies a longer delay in structure formation. As a result, one can deduce from Fig. 3 (left panel) that, for molecular cooling ($T_{\rm vir}^{\rm min} = 10^3$ K), the scattering cross section must be below $10^{-10}\sigma_T \times (m_{\rm DM}/{\rm GeV})$. If one assumes instead that the only efficient cooling mechanism is atomic cooling with $T_{\rm vir}^{\rm min} \geq 10^4$ K, the limits on the IDM scattering cross section become much tighter, excluding scattering cross section lower than $10^{-11}\sigma_T \times (m_{\rm DM}/{\rm GeV})$. Our most conservative bound (assuming $f_* = 0.01$) is therefore $\sigma_{\rm IDM} \lesssim 10^{-10}\sigma_T \times (m_{\rm DM}/{\rm GeV})$. This constraint is stronger than

the 95% CL upper limit of $\sigma_{\rm IDM} < 8 \times 10^{-10}\sigma_T \times (m_{\rm DM}/{\rm GeV})$ reported in Ref. [60], based on observations of Milky Way satellite galaxy number counts and assuming a mass for our galaxy of $M_{\rm MW} = 2.6 \times 10^{12}\ M_\odot$.

Notice that the Lyman-α coupling coefficient x_α is directly proportional to the fraction of baryons converted into stars (f_*), here considered as constant. The left (right) panels of Fig. 3 have been simulated with $f_* = 0.01$ ($f_* = 0.03$). Notice that larger values of f_* increase the Lyman-α coupling at a fixed redshift, weakening the bound on IDM scenarios resulting from Eq. (3.1). In the case of $f_* = 0.03$, the limits quoted above are translated into $\sigma_{\rm IDM} \lesssim 10^{-9}\sigma_T \times (m_{\rm DM}/{\rm GeV})$ and $\sigma_{\rm IDM} \lesssim 10^{-10}\sigma_T \times (m_{\rm DM}/{\rm GeV})$ for $T_{\rm vir}^{\rm min} = 10^3$ K and $T_{\rm vir}^{\rm min} = 10^4$ K respectively.

B. Constraints from the position of the absorption minimum in the 21 cm global signature

Another possible avenue to constrain NCDM models using the EDGES observations is based on the location of the minimum of the absorption. Reference [87] imposed that it should be located at a redshift higher than $z = 17.2$ and studied the resulting bounds on a large set of NCDM models. We show in the bottom panels of Fig. 3 the effect of the IDM scenario considered here on the global sky-averaged 21 cm brightness temperature obtained by means of Eq. (2.1).

Let us focus first in the $f_* = 0.01$ case (i.e., left panel). Considering atomic cooling (dotted curves with $T_{\rm vir}^{\rm min} = 10^4$ K), it appears that for scattering cross sections larger than $\sim 10^{-11}\sigma_T \times (m_{\rm DM}/{\rm GeV})$ the absorption minimum takes place at redshifts lower than $z = 17.2$. Such cross sections should therefore be regarded as disfavored. Considering molecular cooling softens this constraint by $\sim$ one order of magnitude (see the continuous curves for $T_{\rm vir}^{\rm min} = 10^3$ K). Notice that we have considered a conservative x-ray efficiency of $\zeta_X = 5 \times 10^{56}\ M_\odot^{-1}$ for all curves. Considering lower values of ζ_X will give rise to a later x-ray heating and thus a minimum of absorption located at lower redshifts.

If instead, we consider a larger fraction of baryons converted into stars, $f_* = 0.03$, (see the bottom right panel), and $T_{\rm vir}^{\rm min} = 10^3$ (10^4) K, the limit on the IDM interactions is relaxed, excluding cross sections above $\sim 10^{-9}$ $(10^{-10})\sigma_T \times (m_{\rm DM}/{\rm GeV})$. This is due to the fact that both the x-ray and the Lyman-α emission rates are directly proportional to f_*. Increasing f_* implies an earlier Lyman-α coupling and x-ray heating periods, displacing the minimum of the absorption in the 21 cm signal to a larger redshift.

IV. DISCUSSION AND CONCLUSIONS

Interacting dark matter (IDM) models, in which dark matter is not made out of purely cold, pressureless particles, are an interesting alternative to the standard CDM paradigm and provide a possible avenue to alleviate the so-called small-scale crisis of the ΛCDM. The IDM could be scattering off light or massless degrees of freedom such as photons or neutrinos. Here we have considered the case of dark matter scattering on photons, characterized by the size of the scattering rate over the DM mass, $\sigma_{\rm IDM}/m_{\rm DM}$. The reason for this choice is driven by the availability of a fitting function for the halo mass function relevant for our study. Let us emphasize though that scatterings on neutrinos are expected to give rise to a similar imprint on the 21 cm signal.

Several studies have constrained IDM models based on their suppression of clustering at small scales, exploiting galaxy power spectrum, gravitational lensing, CMB, number of Milky Way dwarf galaxies and Lyman-α forest observations, among others. Here we focus on the imprint of IDM on the 21 cm signal arising from cosmic dawn. Based on a modified version of the 21CMFAST code, our simulations show that IDM delays the formation of haloes capable of star formation, shifting the timing of the 21 cm signal features compared to the standard CDM scenario. A similar effect has been reported in the case of other NCDM models [45,46,60,66]. In this paper, we have considered two possible ways to test the IDM properties against the 21 cm signal. First, following Ref. [89], a significant Lyman-α coupling between the gas and the spin temperature characterizing the 21 cm signal should be present at $z = 20$. Second, as argued in Ref. [87], the location of the absorption minimum in the EDGES signal at $z = 17.2$ implies that any scenario with sufficiently enough delayed structure formation could be discarded.

We have first identified which are the most relevant astrophysical parameters showing large degeneracies with the IDM scattering cross section over the mass $\sigma_{\rm IDM}/m_{\rm DM}$. Namely, the fraction of baryons into stars f_*, the threshold temperature for haloes to host star-forming galaxies $T_{\rm vir}^{\rm min}$ and the x-ray efficiency, ζ_X, have been shown to interfere with the eventual extraction of a nonzero $\sigma_{\rm IDM}$. Fortunately, the parameter ζ_X only plays a significant role in extracting the location of the absorption minimum, and we have adopted the conservative value of $\zeta_X = 5 \times 10^{56}\ M_\odot^{-1}$ (corresponding to an integrated soft band x-ray emissivity of $L_{X<2\,{\rm keV}}/{\rm SFR} = 10^{40.2}$ erg/s/$(M_\odot/{\rm yr})$). We also considered a lower limit on the threshold virial temperature of $T_{\rm vir}^{\rm min} = 10^3$ K (corresponding to molecular cooling) as well as a constant value of $f_* < 0.03$.

Our results are summarized on the left panel of Fig. 4 in the case of $f_* = 0.01$. The top panels shows the Lyman-α coupling coefficient x_α at $z = 20$ for $T_{\rm vir}^{\rm min} = 10^3$ (10^4) K with the top blue (bottom red) curve as a function of the IDM scattering cross section. Notice that the $x_\alpha(z = 20)$ curves saturate to a maximum value at low enough values of the scattering cross section. This corresponds to the limiting $x_\alpha(z = 20)$ value that one would get in the CDM scenario (indicated with the horizontal dotted lines). In

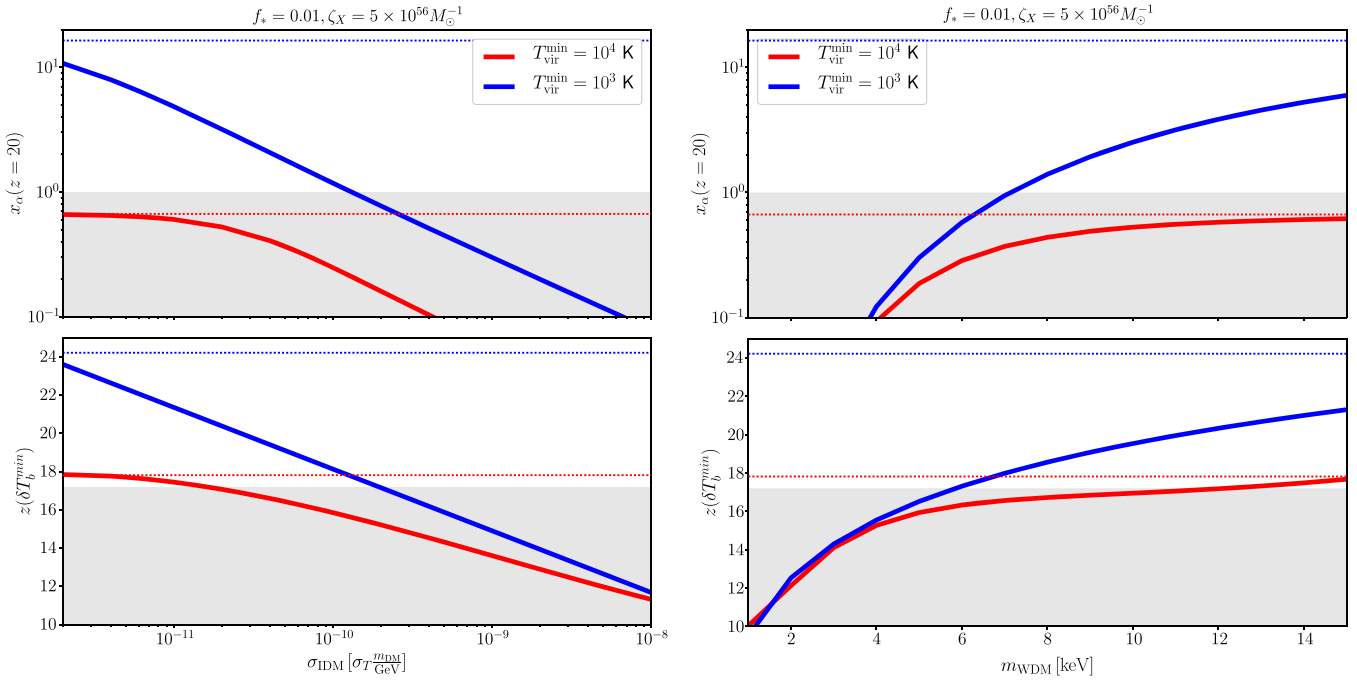

FIG. 4. Left, top (bottom) panel: Lyman-α coupling coefficient x_α at $z = 20$ (redshift of the absorption minimum in the sky-averaged 21 cm brightness temperature) versus the scattering dark matter-photon cross-section for $T_{\rm vir}^{\rm min} = 10^4$ K (atomic cooling) and for $T_{\rm vir}^{\rm min} = 10^3$ K (molecular cooling). Right panels: the same but for WDM models, as a function of the WDM mass $m_{\rm WDM}$. IDM/WDM scenarios lying in the shaded regions are highly disfavoured by the two conditions exploited here, see text for details. We have fixed $f_* = 0.01$ and $\zeta_X = 5 \times 10^{56}\ M_\odot^{-1}$. Dashed lines stand for the results in the CDM scenario.

addition, the shaded region refers to the parameter space in which the condition $x_\alpha(z = 20) > 1$ can not be satisfied and can therefore be considered as disfavored by the condition given by Eq. (3.1). As a result, for $f_* = 0.01$ and $\zeta_X = 5 \times 10^{56}\ M_\odot^{-1}$, a value of $\sigma_{\rm IDM} > 10^{-10}\sigma_T \times (m_{\rm DM}/{\rm GeV})$ fails to satisfy the condition $x_\alpha(z=20)>1$ when considering molecular cooling ($T_{\rm vir}^{\rm min} = 10^3$ K). This improves the previous bound derived on such IDM model in Ref. [60]. When considering higher threshold temperatures for efficient cooling, the bounds gets tighter, disfavoring even the canonical CDM scenario if $T_{\rm vir}^{\rm min} = 10^4$ K. All these limits would be relaxed if the fraction of baryons converted into stars is larger, as it was illustrated in Fig. 3 for $f_* = 0.03$. For instance, for $T_{\rm vir}^{\rm min} = 10^3$ K, the limit would be reduced by one order of magnitude (i.e., $\sigma_{\rm IDM} < 10^{-9}\sigma_T \times (m_{\rm DM}/{\rm GeV})$).

In the bottom left panel of Fig. 4, we show the redshift at which the sky-averaged 21 cm brightness temperature exhibits its minimum of absorption at cosmic dawn, $z(\delta T_b^{\rm min})$, as a function of the IDM scattering cross section. Again $z(\delta T_b^{\rm min})$ saturates for low enough scattering cross-section to a value corresponding to the CDM limit denoted with a dotted horizontal line. The shaded area denotes the region in which this minimum is located below $z = 17.2$. More concretely, in order to derive the curves shown in the bottom panels of Fig. 4, we have fitted the brightness temperature curves obtained from our simulations to the flattened Gaussian shape that the EDGES collaboration uses to model the 21 cm absorption profile [68]. This procedure allows us to extract the central frequency for each possible value of $\sigma_{\rm IDM}/m_{\rm DM}$, $T_{\rm vir}^{\rm min}$ and f_*, and also to constrain the model by imposing that this mean frequency ν_0 of our flattened gaussian fits should lie at frequencies below the lower 99% confidence interval (including estimates of systematic uncertainties) reported by the EDGES collaboration for the $\nu_0 = 78$ MHz parameter.[4] From Fig. 4, the position of the minimum of absorption disfavors the region $\sigma_{\rm IDM} > 10^{-10}\sigma_T \times (m_{\rm DM}/{\rm GeV})$ ($\sigma_{\rm IDM} > 10^{-11}\sigma_T \times (m_{\rm DM}/{\rm GeV})$) for $T_{\rm vir}^{\rm min} = 10^3$ K ($T_{\rm vir}^{\rm min} = 10^4$ K). As in the case of the $x_\alpha(z = 20) > 1$ condition, these limits would be relaxed by one order of magnitude in the case of a value of $f_* = 0.03$. Also, for the astrophysical parameters considered here, we see that the constraints from the Lyman-α coupling condition are typically tighter than those arising from the position of the minimum of absorption. Nevertheless, the uncertainty on the limits derived using the Lyman-α coupling criterion of Eq. (3.1) is more difficult to quantify than the one related to the position of the minimum of absorption. Indeed, using Eq. (3.1), we are not using any specific parameter of the fit

[4]It should be noted that we cannot reproduce precisely the values of other parameters quoted by EDGES of the fits due to the lack of flat bottom and large amplitude in our predictions.

to derive the exclusion region, but a statement on the general shape. Also, notice that there could be a small variation of the limits depending on the redshift at which one assumes that $x_\alpha = 1$. Here $z = 20$ has been taken, but small variations in the range $z = 20 \pm 0.5$ would agree with the δT_b obtained varying the signal parameters within the 99% CL range reported by EDGES. In contrast, the dip-position criterion based on the 99% CL of the location observed by EDGES appears thus to be more robust. Finally, the dip location and x_α criterion are sensitive to different astrophysics parameters. For example, the dip location very much depends on ζ_X while, as can be seen in Fig. 2, x_α is quite insensitive to this parameter at $z \sim 20$. Still, the limits on the DM properties from the two methods show an excellent agreement for $T_{\rm vir}^{\rm min} = 10^3$ K.

Summarizing, for $f_* \simeq 0.01$, $\zeta_X < 5 \times 10^{56}\ M_\odot^{-1}$ and $T_{\rm vir}^{\rm min} > 10^3$ K, the bounds on $\sigma_{\rm IDM}/m_{\rm DM}$ derived in this work imply an order of magnitude improvement over the most constraining existing limits in the literature [2,60]. Larger values of f_* may compromise these upgraded limits. In order to ease the comparison to other studies on NCDM scenarios, we provide the results obtained following the same methodology in a thermal warm dark matter scenario involving light dark matter particles with a mass $m_{\rm WDM}$ of a few keV. The prescription considered here to describe the suppression of the halo mass function at small halo masses is given in the Appendix A. We show the obtained dependence of $x_\alpha(z = 20)$ and $z(\delta T_b^{\rm min})$ in the right panel of Fig. 4. From this figure with $f_* = 0.01$ and $\zeta_X = 5 \times 10^{56}\ M_\odot^{-1}$, we can infer a lower limit in the WDM mass around $m_{\rm WDM} > 6$ keV ($m_{\rm WDM} > 12$ keV) if $T_{\rm vir}^{\rm min} = 10^3$ K ($T_{\rm vir}^{\rm min} = 10^4$ K). These tight limits are similar to those derived in Refs. [87,89] for slightly different WDM implementations and astrophysical parameters. As a final comment, it should be noted that IDM cross sections or WDM masses in these allowed regions could be not sufficient to solve the small-scale problems, since they predict a similar amount of substructures than the CDM case (see e.g., Table II of [143] for the WDM prescription). However, increasing f_* to 0.03 would relax the constraints by about one order of magnitude (recall the discussion about Fig. 3), being therefore these NCDM scenarios still suitable to deal with the subgalactic issues.

ACKNOWLEDGMENTS

L. L. H. is supported by the FNRS, by the Strategic Research Program *High Energy Physics* and by the Research Council of the Vrije Universiteit Brussel. O. M. and P. V. D. are supported by PROMETEO II/2014/050, by the Spanish MINECO Grants No. FPA2014–57816-P, No. FPA2017-85985-P, and No. SEV-2014-0398 and by the European Union's Horizon 2020 research and innovation program under the Marie Sklodowska-Curie Grant Agreements No. 690575 and 674896.

APPENDIX A: HALO MASS FUNCTIONS

The halo mass function, that counts the number of haloes per unit halo mass and volume at a given redshift, can be written as [144]

$$\frac{dn}{dM} = -\frac{1}{2}\frac{\rho_m}{M^2} f(\nu) \frac{d\ln\sigma^2}{d\ln M}, \tag{A1}$$

where n is the halo number density, $\rho_m = \Omega_m \rho_c$ is the average matter density in the Universe at $z = 0$ and $\sigma^2 = \sigma^2(M, z)$ is the variance of density perturbations, which is a function of the halo mass M and redshift. The first-crossing distribution, $f(\nu)$, is expected to be a universal function of $\nu \equiv \delta_c^2/\sigma^2(M, z)$, with $\delta_c = 1.686$, the linearly extrapolated density for collapse at $z = 0$. The Sheth-Tormen (ST) first-crossing distribution reads as [145–147]:

$$f(\nu) = A\sqrt{\frac{2q\nu}{\pi}}(1 + (q\nu)^{-p})e^{-q\nu/2}, \tag{A2}$$

with $p = 0.3$, $q = 0.707$ and $A = 0.3222$. For the standard CDM scenario, we consider this first-crossing distribution. The variance at $z = 0$, $\sigma(M) \equiv \sigma(M, z = 0)$, at a given scale R can be expressed as

$$\sigma_X^2(M(R)) = \int \frac{d^3k}{(2\pi)^3} P_X(k) W^2(kR), \tag{A3}$$

where $P_X(k)$ is the linear power spectrum at $z = 0$ for a given $X = \{\text{CDM, IDM or WDM}\}$ cosmology and W is the Fourier transform of a filter function that we consider to be a top-hat (TH) function in real space (see, e.g., [16,87] for the possibility of using a sharp-k window function for NCDM). The redshift dependence is driven by the linear growth function, $D(z)$ normalized to 1 at $z = 0$, so that the root-mean-square (rms) density fluctuation is $\sigma(M, z) = \sigma(M, z = 0)D(z)$.

The transfer function T_X for a NCDM scenario X is defined as

$$P_X(k) = P_{\rm CDM}(k) T_X^2(k), \tag{A4}$$

where $P_{\rm CDM}(k)$ is the linear power spectrum in ΛCDM. Here we use the prescription of Refs. [14,94]:

$$T_X(k) = (1 + (\alpha_X k)^{2\mu})^{-5/\mu}, \tag{A5}$$

where $\mu = 1.2$ is a dimensionless exponent and α_X is a breaking scale. The latter takes the form:

$$\alpha_{\rm WDM} = 0.048 \left(\frac{\rm keV}{m_{\rm WDM}}\right)^{1.15} \left(\frac{\Omega_{\rm WDM}}{0.4}\right)^{0.15} \left(\frac{h}{0.65}\right)^{1.3} {\rm Mpc}/h, \tag{A6}$$

$$\alpha_{\gamma\mathrm{DM}} = 0.073\left[10^8\left(\frac{\sigma_{\mathrm{IDM}}}{\sigma_T}\right)\left(\frac{\mathrm{GeV}}{m_{\mathrm{DM}}}\right)\right]^{0.48}\left(\frac{\Omega_{\mathrm{WDM}}}{0.4}\right)^{0.15} \times \left(\frac{h}{0.65}\right)^{1.3}\mathrm{Mpc}/h. \quad \text{(A7)}$$

for WDM scenarios [3,100] and IDM involving dark matter-photon scattering [14] respectively. For DM-neutrino interactions, described with the same parametrization of the transfer function, one gets a breaking scale $\alpha_{\nu\mathrm{DM}} \simeq 0.8 \times \alpha_{\gamma\mathrm{DM}}$ for a fixed value of the scattering cross section [3].

The halo mass function defined as in Eq. (A1) is well suited for CDM but it needs to be adapted for the NCDM case. In order to match the results from N-body simulations, the WDM halo mass function can be expressed as [100]

$$\frac{dn^{\mathrm{WDM}}}{dM} = \left(1 + \frac{M_{\mathrm{hm}}}{bM}\right)^a \frac{dn^{\mathrm{ST,WDM}}}{dM}, \quad \text{(A8)}$$

where an additional mass-dependent correction to the standard ST formalism appears. We use $a = -0.6$ and $b = 0.5$, as obtained in [3,90]. The function $\frac{dn^{\mathrm{ST,WDM}}}{dM}$ in Eq. (A8) refers to the halo mass function obtained with a ST first-crossing distribution, as defined in Eq. (A2), and a linear matter power spectrum corresponding to the WDM case. In order to describe the suppression in the linear regime, one can consider the half-mode mass M_{hm}, defined as the mass scale for which $T_X/T_{\mathrm{CDM}} = 1/2$ (i.e., $P_X/P_{\mathrm{CDM}} = 1/4$). Using the general fit to the transfer function, Eq. (A5), the half-mode mass M_{hm} can be easily derived as

$$M_{\mathrm{hm}} \equiv \frac{4\pi}{3}\rho_m(\pi\alpha_X)^3(2^{\mu/5} - 1)^{-3/(2\mu)}. \quad \text{(A9)}$$

For what concerns the IDM models, the number of low-mass structures appears to be larger than in WDM scenarios [3] (see also [7]). In order to reproduce the IDM results for masses below the half-mode mass, an extra mass-dependent correction must be introduced to the halo mass function [90]:

$$\frac{dn^{\mathrm{IDM}}}{dM} = \left(1 + \frac{M_{\mathrm{hm}}}{bM}\right)^a \left(1 + \frac{M_{\mathrm{hm}}}{gM}\right)^c \frac{dn^{\mathrm{ST,CDM}}}{dM}, \quad \text{(A10)}$$

with $a = -1$, $b = 0.33$, $g = 1$, $c = 0.6$ and $\frac{dn^{\mathrm{ST,CDM}}}{dM}$ refers to the standard ST first-crossing distribution as defined in Eq. (A2) with the CDM linear power spectrum for the variance of density perturbations.

APPENDIX B: LYMAN-α EMISSIVITY

The Lyman-α flux from direct stellar emission of UV photons, $J_{\alpha\star}$, is given by the sum over the Lyman-n levels which can lead to a $2p \to 1s$ transition through a decaying cascade. Due to the optical thickness of the IGM, photons which redshift to a Lyman resonance are absorbed by the medium. A photon which reaches a Lyman-n resonance at redshift z has to be emitted at a redshift below $1 + z_{\mathrm{max},n} = \frac{1-(n+1)^{-2}}{1-n^{-2}}(1+z)$. If $f_{\mathrm{rec}}(n)$ is the recycled fraction of the level n, i.e., the probability of generating a Lyman-α photon from the n level [148], the total Lyman-α flux can be written as

$$J_{\alpha\star} = \frac{c(1+z)^2}{4\pi}\sum_{n=2}^{n_{\mathrm{max}}} f_{\mathrm{rec}}(n)\int_z^{z_{\mathrm{max},n}} dz' \frac{\epsilon_\alpha(\nu'_n, z')}{H(z')}, \quad \text{(B1)}$$

where the emission frequency is $\nu'_n = \nu_n \frac{1+z'}{1+z}$, being $\nu_n = \nu_{\mathrm{LL}}(1 - n^{-2})$ and ν_{LL} the Lyman limit frequency. The comoving emissivity ϵ_α can be written as proportional to the comoving star formation rate $\dot{\rho}_{\star,0}$:

$$\epsilon_\alpha(\nu, z) = \varepsilon(\nu)\frac{\dot{\rho}_{\star,0}(z)}{\mu m_p} = \varepsilon(\nu) f_* \bar{n}_{b,0}\dot{f}_{\mathrm{coll}}(z), \quad \text{(B2)}$$

where $\bar{n}_{b,0}$ is the comoving number density of baryons. Assuming that only Population-II stars contribute to this emissivity, the spectral distribution $\varepsilon(\nu)$ is given by a separate power law between each Lyman-n and Lyman-$n+1$ levels:

$$\varepsilon(\nu) = N_n \frac{(\beta_n + 1)\nu_\alpha^{\beta_n}}{(\nu_{n+1}^{\beta_n+1} - \nu_n^{\beta_n+1})}\left(\frac{\nu}{\nu_\alpha}\right)^{\beta_n}, \quad \text{(B3)}$$

for $\nu_n \le \nu \le \nu_{n+1}$, with N_n the number of photons emitted between the n and $n+1$ resonances and β_n the spectral index [122]. The function above is normalized as $\int_{\nu_n}^{\nu_{n+1}} d\nu\varepsilon(\nu) = N_n$, with $\int_{\nu_\alpha}^{\nu_{\mathrm{LL}}} d\nu\varepsilon(\nu) = \sum_n N_n \simeq 9690$ the total number of photons emitted between the Lyman-α and the Lyman limit. Although we keep this normalization as constant through our analysis, notice that changes in the number of photons which contribute to the Lyman-α flux could have a deep impact in the 21 cm signal [141].

[1] C. Boehm, H. Mathis, J. Devriendt, and J. Silk, Mon. Not. R. Astron. Soc. **360**, 282 (2005).
[2] C. Bœhm, J. A. Schewtschenko, R. J. Wilkinson, C. M. Baugh, and S. Pascoli, Mon. Not. R. Astron. Soc. **445**, L31 (2014).
[3] J. A. Schewtschenko, R. J. Wilkinson, C. M. Baugh, C. Bœhm, and S. Pascoli, Mon. Not. R. Astron. Soc. **449**, 3587 (2015).
[4] J. A. Schewtschenko, C. M. Baugh, R. J. Wilkinson, C. Bœhm, S. Pascoli, and T. Sawala, Mon. Not. R. Astron. Soc. **461**, 2282 (2016).
[5] F.-Y. Cyr-Racine, R. de Putter, A. Raccanelli, and K. Sigurdson, Phys. Rev. D **89**, 063517 (2014).
[6] M. R. Buckley, J. Zavala, F.-Y. Cyr-Racine, K. Sigurdson, and M. Vogelsberger, Phys. Rev. D **90**, 043524 (2014).
[7] M. Vogelsberger, J. Zavala, F.-Y. Cyr-Racine, C. Pfrommer, T. Bringmann, and K. Sigurdson, Mon. Not. R. Astron. Soc. **460**, 1399 (2016).
[8] F.-Y. Cyr-Racine, K. Sigurdson, J. Zavala, T. Bringmann, M. Vogelsberger, and C. Pfrommer, Phys. Rev. D **93**, 123527 (2016).
[9] L. G. van den Aarssen, T. Bringmann, and C. Pfrommer, Phys. Rev. Lett. **109**, 231301 (2012).
[10] T. Bringmann, H. T. Ihle, J. Kersten, and P. Walia, Phys. Rev. D **94**, 103529 (2016).
[11] T. Binder, L. Covi, A. Kamada, H. Murayama, T. Takahashi, and N. Yoshida, J. Cosmol. Astropart. Phys. 11 (2016) 043.
[12] A. Kamada and T. Takahashi, J. Cosmol. Astropart. Phys. 01 (2018) 047.
[13] C. Bœhm, P. Fayet, and R. Schaeffer, Phys. Lett. B **518**, 8 (2001).
[14] C. Bœhm, A. Riazuelo, S. H. Hansen, and R. Schaeffer, Phys. Rev. D **66**, 083505 (2002).
[15] C. Bœhm and R. Schaeffer, Astron. Astrophys. **438**, 419 (2005).
[16] R. Murgia, A. Merle, M. Viel, M. Totzauer, and A. Schneider, J. Cosmol. Astropart. Phys. 11 (2017) 046.
[17] J. S. Bullock and M. Boylan-Kolchin, Annu. Rev. Astron. Astrophys. **55**, 343 (2017).
[18] M. Viel, G. D. Becker, J. S. Bolton, and M. G. Haehnelt, Phys. Rev. D **88**, 043502 (2013).
[19] M. Viel, J. Lesgourgues, M. G. Haehnelt, S. Matarrese, and A. Riotto, Phys. Rev. D **71**, 063534 (2005).
[20] U. Seljak, A. Makarov, P. McDonald, and H. Trac, Phys. Rev. Lett. **97**, 191303 (2006).
[21] M. Viel, J. Lesgourgues, M. G. Haehnelt, S. Matarrese, and A. Riotto, Phys. Rev. Lett. **97**, 071301 (2006).
[22] G. Mangano, A. Melchiorri, P. Serra, A. Cooray, and M. Kamionkowski, Phys. Rev. D **74**, 043517 (2006).
[23] M. Viel, G. D. Becker, J. S. Bolton, M. G. Haehnelt, M. Rauch, and W. L. W. Sargent, Phys. Rev. Lett. **100**, 041304 (2008).
[24] A. Boyarsky, J. Lesgourgues, O. Ruchayskiy, and M. Viel, J. Cosmol. Astropart. Phys. 05 (2009) 012.
[25] P. Serra, F. Zalamea, A. Cooray, G. Mangano, and A. Melchiorri, Phys. Rev. D **81**, 043507 (2010).
[26] S. D. McDermott, H.-B. Yu, and K. M. Zurek, Phys. Rev. D **83**, 063509 (2011).
[27] R. J. Wilkinson, J. Lesgourgues, and C. Bœhm, J. Cosmol. Astropart. Phys. 04 (2014) 026.
[28] A. D. Dolgov, S. L. Dubovsky, G. I. Rubtsov, and I. I. Tkachev, Phys. Rev. D **88**, 117701 (2013).
[29] R. J. Wilkinson, C. Bœhm, and J. Lesgourgues, J. Cosmol. Astropart. Phys. 05 (2014) 011.
[30] A. Schneider, Mon. Not. R. Astron. Soc. **451**, 3117 (2015).
[31] M. Escudero, O. Mena, A. C. Vincent, R. J. Wilkinson, and C. Bœhm, J. Cosmol. Astropart. Phys. 09 (2015) 034.
[32] Y. Ali-Haïmoud, J. Chluba, and M. Kamionkowski, Phys. Rev. Lett. **115**, 071304 (2015).
[33] J. Baur, N. Palanque-Delabrouille, C. Yèche, C. Magneville, and M. Viel, J. Cosmol. Astropart. Phys. 08 (2016) 012.
[34] R. Diamanti, S. Ando, S. Gariazzo, O. Mena, and C. Weniger, J. Cosmol. Astropart. Phys. 06 (2017) 008.
[35] V. Irsic *et al.*, Phys. Rev. D **96**, 023522 (2017).
[36] C. Yèche, N. Palanque-Delabrouille, J. Baur, and H. du Mas des Bourboux, J. Cosmol. Astropart. Phys. 06 (2017) 047.
[37] S. Gariazzo, M. Escudero, R. Diamanti, and O. Mena, Phys. Rev. D **96**, 043501 (2017).
[38] J. A. D. Diacoumis and Y. Y. Y. Wong, J. Cosmol. Astropart. Phys. 09 (2017) 011.
[39] E. Di Valentino, C. Bœhm, E. Hivon, and F. R. Bouchet, Phys. Rev. D **97**, 043513 (2018).
[40] A. O.-D. Campo, C. Bœhm, S. Palomares-Ruiz, and S. Pascoli, Phys. Rev. D **97**, 075939 (2018).
[41] J. Stadler and C. Bœhm, J. Cosmol. Astropart. Phys. 10 (2018) 009.
[42] A. D. Rivero, C. Dvorkin, F.-Y. Cyr-Racine, J. Zavala, and M. Vogelsberger, Phys. Rev. D **98**, 103517 (2018).
[43] M. R. Lovell, J. Zavala, M. Vogelsberger, X. Shen, F.-Y. Cyr-Racine, C. Pfrommer, K. Sigurdson, M. Boylan-Kolchin, and A. Pillepich, Mon. Not. R. Astron. Soc. **477**, 2886 (2018).
[44] P. Dayal, A. Mesinger, and F. Pacucci, Astrophys. J. **806**, 67 (2015).
[45] S. Bose, C. S. Frenk, J. Hou, C. G. Lacey, and M. R. Lovell, Mon. Not. R. Astron. Soc. **463**, 3848 (2016).
[46] L. Lopez-Honorez, O. Mena, S. Palomares-Ruiz, and P. Villanueva-Domingo, Phys. Rev. D **96**, 103539 (2017).
[47] R. Barkana, Z. Haiman, and J. P. Ostriker, Astrophys. J. **558**, 482 (2001).
[48] N. Yoshida, A. Sokasian, L. Hernquist, and V. Springel, Astrophys. J. **591**, L1 (2003).
[49] R. S. Somerville, J. S. Bullock, and M. Livio, Astrophys. J. **593**, 616 (2003).
[50] B. Yue and X. Chen, Astrophys. J. **747**, 127 (2012).
[51] F. Pacucci, A. Mesinger, and Z. Haiman, Mon. Not. R. Astron. Soc. **435**, L53 (2013).
[52] A. Mesinger, A. Ewall-Wice, and J. Hewitt, Mon. Not. R. Astron. Soc. **439**, 3262 (2014).
[53] C. Schultz, J. Oñorbe, K. N. Abazajian, and J. S. Bullock, Mon. Not. R. Astron. Soc. **442**, 1597 (2014).
[54] A. Lapi and L. Danese, J. Cosmol. Astropart. Phys. 09 (2015) 003.
[55] S. Bose, W. A. Hellwing, C. S. Frenk, A. Jenkins, M. R. Lovell, J. C. Helly, B. Li, V. Gonzalez-Perez, and L. Gao, Mon. Not. R. Astron. Soc. **464**, 4520 (2017).
[56] P. S. Corasaniti, S. Agarwal, D. J. E. Marsh, and S. Das, Phys. Rev. D **95**, 083512 (2017).

[57] N. Menci, A. Grazian, M. Castellano, and N. G. Sanchez, Astrophys. J. **825**, L1 (2016).
[58] P. Villanueva-Domingo, N. Y. Gnedin, and O. Mena, Astrophys. J. **852**, 139 (2018).
[59] S. Das, R. Mondal, V. Rentala, and S. Suresh, J. Cosmol. Astropart. Phys. 08 (2018) 045.
[60] M. Escudero, L. Lopez-Honorez, O. Mena, S. Palomares-Ruiz, and P. Villanueva-Domingo, J. Cosmol. Astropart. Phys. 06 (2018) 007.
[61] P. Dayal, T. R. Choudhury, V. Bromm, and F. Pacucci, Astrophys. J. **836**, 16 (2017).
[62] P. Dayal, T. R. Choudhury, F. Pacucci, and V. Bromm, Mon. Not. R. Astron. Soc. **472**, 4414 (2017).
[63] A. Harada and A. Kamada, J. Cosmol. Astropart. Phys. 01 (2016) 031.
[64] A. Kamada, K. T. Inoue, and T. Takahashi, Phys. Rev. D **94**, 023522 (2016).
[65] A. Kamada, K. Kohri, T. Takahashi, and N. Yoshida, Phys. Rev. D **95**, 023502 (2017).
[66] M. Sitwell, A. Mesinger, Y.-Z. Ma, and K. Sigurdson, Mon. Not. R. Astron. Soc. **438**, 2664 (2014).
[67] I. P. Carucci, F. Villaescusa-Navarro, M. Viel, and A. Lapi, J. Cosmol. Astropart. Phys. 07 (2015) 047.
[68] J. D. Bowman, A. E. E. Rogers, R. A. Monsalve, T. J. Mozdzen, and N. Mahesh, Nature (London) **555**, 67 (2018).
[69] A. Berlin, D. Hooper, G. Krnjaic, and S. D. McDermott, Phys. Rev. Lett. **121**, 011102 (2018).
[70] G. D'Amico, P. Panci, and A. Strumia, Phys. Rev. Lett. **121**, 011103 (2018).
[71] H. Liu and T. R. Slatyer, Phys. Rev. D **98**, 023501 (2018).
[72] A. Mitridate and A. Podo, J. Cosmol. Astropart. Phys. 05 (2018) 069.
[73] M. Valdés, C. Evoli, A. Mesinger, A. Ferrara, and N. Yoshida, Mon. Not. R. Astron. Soc. **429**, 1705 (2013).
[74] C. Evoli, A. Mesinger, and A. Ferrara, J. Cosmol. Astropart. Phys. 11 (2014) 024.
[75] L. Lopez-Honorez, O. Mena, A. Moliné, S. Palomares-Ruiz, and A. C. Vincent, J. Cosmol. Astropart. Phys. 08 (2016) 004.
[76] M. Pospelov, J. Pradler, J. T. Ruderman, and A. Urbano, Phys. Rev. Lett. **121**, 031103 (2018).
[77] D. Aristizabal Sierra and C. S. Fong, Phys. Lett. B **784**, 130 (2018).
[78] K. K. Boddy, V. Gluscevic, V. Poulin, E. D. Kovetz, M. Kamionkowski, and R. Barkana, Phys. Rev. D **98**, 123506 (2018).
[79] E. D. Kovetz, V. Poulin, V. Gluscevic, K. K. Boddy, R. Barkana, and M. Kamionkowski, Phys. Rev. D **98**, 103529 (2018).
[80] R. Barkana, N. J. Outmezguine, D. Redigolo, and T. Volansky, Phys. Rev. D **98**, 103005 (2018).
[81] R. Barkana, Nature (London) **555**, 71 (2018).
[82] A. Hektor, G. Hütsi, L. Marzola, and V. Vaskonen, Phys. Lett. B **785**, 429 (2018).
[83] A. Hektor, G. Hütsi, L. Marzola, M. Raidal, V. Vaskonen, and H. Veermäe, Phys. Rev. D **98**, 023503 (2018).
[84] S. Fraser *et al.*, Phys. Lett. B **785**, 159 (2018).
[85] R. Hills, G. Kulkarni, P. D. Meerburg, and E. Puchwein, Nature (London) **564**, E32 (2018).
[86] R. F. Bradley, K. Tauscher, D. Rapetti, and J. O. Burns, arXiv:1810.09015.
[87] A. Schneider, Phys. Rev. D **98**, 063021 (2018).
[88] M. Safarzadeh, E. Scannapieco, and A. Babul, Astrophys. J. **859**, L18 (2018).
[89] A. Lidz and L. Hui, Phys. Rev. D **98**, 023011 (2018).
[90] Á. Moliné, J. A. Schewtschenko, S. Palomares-Ruiz, C. Bœhm, and C. M. Baugh, J. Cosmol. Astropart. Phys. 08 (2016) 069.
[91] J. A. Schewtschenko, Cosmological simulations with Dark Matter from beyond the Standard Model, Ph.D. thesis, Durham U., 2016.
[92] C. Dvorkin, K. Blum, and M. Kamionkowski, Phys. Rev. D **89**, 023519 (2014).
[93] N. Vinyoles and H. Vogel, J. Cosmol. Astropart. Phys. 03 (2016) 002.
[94] P. Bode, J. P. Ostriker, and N. Turok, Astrophys. J. **556**, 93 (2001).
[95] A. Knebe, J. E. G. Devriendt, A. Mahmood, and J. Silk, Mon. Not. R. Astron. Soc. **329**, 813 (2002).
[96] P. Colin, O. Valenzuela, and V. Avila-Reese, Astrophys. J. **673**, 203 (2008).
[97] J. Zavala, Y. P. Jing, A. Faltenbacher, G. Yepes, Y. Hoffman, S. Gottlöber, and B. Catinella, Astrophys. J. **700**, 1779 (2009).
[98] R. E. Smith and K. Markovic, Phys. Rev. D **84**, 063507 (2011).
[99] M. R. Lovell, V. Eke, C. S. Frenk, L. Gao, A. Jenkins, T. Theuns, J. Wang, S. D. M. White, A. Boyarsky, and O. Ruchayskiy, Mon. Not. R. Astron. Soc. **420**, 2318 (2012).
[100] A. Schneider, R. E. Smith, A. V. Macciò, and B. Moore, Mon. Not. R. Astron. Soc. **424**, 684 (2012).
[101] E. Polisensky and M. Ricotti, Mon. Not. R. Astron. Soc. **437**, 2922 (2014).
[102] M. R. Lovell, C. S. Frenk, V. R. Eke, A. Jenkins, L. Gao, and T. Theuns, Mon. Not. R. Astron. Soc. **439**, 300 (2014).
[103] R. Kennedy, C. Frenk, S. Cole, and A. Benson, Mon. Not. R. Astron. Soc. **442**, 2487 (2014).
[104] C. Destri, H. J. de Vega, and N. G. Sánchez, Phys. Rev. D **88**, 083512 (2013).
[105] R. E. Angulo, O. Hahn, and T. Abel, Mon. Not. R. Astron. Soc. **434**, 3337 (2013).
[106] A. J. Benson, A. Farahi, S. Cole, L. A. Moustakas, A. Jenkins, M. Lovell, R. Kennedy, J. Helly, and C. Frenk, Mon. Not. R. Astron. Soc. **428**, 1774 (2013).
[107] A. Kamada, N. Yoshida, K. Kohri, and T. Takahashi, J. Cosmol. Astropart. Phys. 03 (2013) 008.
[108] M. R. Lovell, S. Bose, A. Boyarsky, S. Cole, C. S. Frenk, V. Gonzalez-Perez, R. Kennedy, O. Ruchayskiy, and A. Smith, Mon. Not. R. Astron. Soc. **461**, 60 (2016).
[109] A. D. Ludlow, S. Bose, R. E. Angulo, L. Wang, W. A. Hellwing, J. F. Navarro, S. Cole, and C. S. Frenk, Mon. Not. R. Astron. Soc. **460**, 1214 (2016).
[110] L. Wang, V. Gonzalez-Perez, L. Xie, A. P. Cooper, C. S. Frenk, L. Gao, W. A. Hellwing, J. Helly, M. R. Lovell, and L. Jiang, Mon. Not. R. Astron. Soc. **468**, 4579 (2017).
[111] M. R. Lovell, V. Gonzalez-Perez, S. Bose, A. Boyarsky, S. Cole, C. S. Frenk, and O. Ruchayskiy, Mon. Not. R. Astron. Soc. **468**, 2836 (2017).
[112] T. Nakama, J. Chluba, and M. Kamionkowski, Phys. Rev. D **95**, 121302 (2017).

[113] P. Madau, A. Meiksin, and M. J. Rees, Astrophys. J. **475**, 429 (1997).
[114] S. Furlanetto, S. P. Oh, and F. Briggs, Phys. Rep. **433**, 181 (2006).
[115] J. R. Pritchard and A. Loeb, Rep. Prog. Phys. **75**, 086901 (2012).
[116] S. R. Furlanetto, in *Understanding the Epoch of Cosmic Reionization: Challenges and Progress*, edited by A. Mesinger (Springer International Publishing, Scuola Normale Superiore, Pisa PI, Italy, 2016), Vol. 423, pp. 247–280.
[117] C. M. Hirata, Mon. Not. R. Astron. Soc. **367**, 259 (2006).
[118] S. A. Wouthuysen, Astrophys. J. **57**, 31 (1952).
[119] G. B. Field, Proc. IRE **46**, 240 (1958).
[120] X.-L. Chen and J. Miralda-Escude, Astrophys. J. **602**, 1 (2004).
[121] A. Mesinger, S. Furlanetto, and R. Cen, Mon. Not. R. Astron. Soc. **411**, 955 (2011).
[122] R. Barkana and A. Loeb, Astrophys. J. **626**, 1 (2005).
[123] R. S. de Souza, A. Mesinger, A. Ferrara, Z. Haiman, R. Perna, and N. Yoshida, Mon. Not. R. Astron. Soc. **432**, 3218 (2013).
[124] Á. Moliné, M. A. Sánchez-Conde, S. Palomares-Ruiz, and F. Prada, Mon. Not. R. Astron. Soc. **466**, 4974 (2017).
[125] R. Barkana and A. Loeb, Phys. Rep. **349**, 125 (2001).
[126] A. E. Evrard, Astrophys. J. **363**, 349 (1990).
[127] A. Blanchard, D. Valls-Gabaud, and G. A. Mamon, Astron. Astrophys. **264**, 365 (1992).
[128] M. Tegmark, J. Silk, M. J. Rees, A. Blanchard, T. Abel, and F. Palla, Astrophys. J. **474**, 1 (1997).
[129] Z. Haiman, T. Abel, and M. J. Rees, Astrophys. J. **534**, 11 (2000).
[130] B. Ciardi, A. Ferrara, F. Governato, and A. Jenkins, Mon. Not. R. Astron. Soc. **314**, 611 (2000).
[131] J. H. Wise and T. Abel, Astrophys. J. **671**, 1559 (2007).
[132] J. H. Wise, V. G. Demchenko, M. T. Halicek, M. L. Norman, M. J. Turk, T. Abel, and B. D. Smith, Mon. Not. R. Astron. Soc. **442**, 2560 (2014).
[133] H. Xu, J. H. Wise, M. L. Norman, K. Ahn, and B. W. O'Shea, Astrophys. J. **833**, 84 (2016).
[134] X. Ma, P. F. Hopkins, S. Garrison-Kimmel, C.-A. Faucher-Giguère, E. Quataert, M. Boylan-Kolchin, C. C. Hayward, R. Feldmann, and D. Kereš, Mon. Not. R. Astron. Soc. **478**, 1694 (2018).
[135] J. Rosdahl, H. Katz, J. Blaizot, T. Kimm, L. Michel-Dansac, T. Garel, M. Haehnelt, P. Ocvirk, and R. Teyssier, Mon. Not. R. Astron. Soc. **479**, 994 (2018).
[136] N. Mashian, P. A. Oesch, and A. Loeb, Mon. Not. R. Astron. Soc. **455**, 2101 (2016).
[137] N. Leite, C. Evoli, M. D'Angelo, B. Ciardi, G. Sigl, and A. Ferrara, Mon. Not. R. Astron. Soc. **469**, 416 (2017).
[138] B. Greig and A. Mesinger, Mon. Not. R. Astron. Soc. **449**, 4246 (2015).
[139] S. Mineo, M. Gilfanov, and R. Sunyaev, Mon. Not. R. Astron. Soc. **426**, 1870 (2012).
[140] R. A. Monsalve, B. Greig, J. D. Bowman, A. Mesinger, A. E. E. Rogers, T. J. Mozdzen, N. S. Kern, and N. Mahesh, Astrophys. J. **863**, 11 (2018).
[141] S. Witte, P. Villanueva-Domingo, S. Gariazzo, O. Mena, and S. Palomares-Ruiz, Phys. Rev. D **97**, 103533 (2018).
[142] A. A. Kaurov, T. Venumadhav, L. Dai, and M. Zaldarriaga, Astrophys. J. **864**, L15 (2018).
[143] S. Y. Kim, A. H. G. Peter, and J. R. Hargis, Phys. Rev. Lett. **121**, 211302 (2018).
[144] W. H. Press and P. Schechter, Astrophys. J. **187**, 425 (1974).
[145] R. K. Sheth and G. Tormen, Mon. Not. R. Astron. Soc. **308**, 119 (1999).
[146] R. K. Sheth, H. J. Mo, and G. Tormen, Mon. Not. R. Astron. Soc. **323**, 1 (2001).
[147] R. K. Sheth and G. Tormen, Mon. Not. R. Astron. Soc. **329**, 61 (2002).
[148] J. R. Pritchard and S. R. Furlanetto, Mon. Not. R. Astron. Soc. **367**, 1057 (2006).